LA-UR-02-2954

Approved for public release; distribution is unlimited.

c.1

Title: PROPAGATION STUDIES OF METASTABLE INTERMOLECULAR COMPOSITES (MIC)

Author(s):
S.F. Son
J.R. Busse
B.W. Asay
P.D. Peterson
J.T. Mang
B. Bockmon
M.L. Pantoya

Submitted to:
The 29th International Pyrotechnics Seminar
The Major International Forum for Pyrotechnics
Westminster, CO, USA
July 14-19, 2002

Los Alamos
NATIONAL LABORATORY

PROPAGATION STUDIES OF METASTABLE INTERMOLECULAR COMPOSITES (MIC)

S. F. Son[1], J. R. Busse[1], B. W. Asay[1], P. D. Peterson[1], J. T. Mang[1]
B. Bockmon[2] and M. L. Pantoya[2]

[1] Los Alamos National Laboratory, Los Alamos, New Mexico, 87545
[2] Mechanical Engineering Department, Texas Tech University, Lubbock, Texas, 79409
son@lanl.gov

ABSTRACT

Thermite materials are attractive energetic materials because the reactions are highly exothermic, have high energy densities, and high temperatures of combustion. However, the application of thermite materials has been limited because of the relative slow release of energy compared to other energetic materials. Engineered nano-scale composite energetic materials, such as Al/MoO_3, show promise for additional energetic material applications because they can react very rapidly. The composite material studied in this work consists of tailored, ultra-fine grain (30-200 nm diameter) aluminum particles that dramatically increase energy release rates of these thermite materials. These reactant clusters of fuel and oxidizer particles are in nearly atomic scale proximity to each other but are constrained from reaction until triggered. Despite the growing importance of nano-scale energetic materials, even the most basic combustion characteristics of these materials have not been thoroughly studied. This paper reports initial studies of the ignition and combustion of metastable intermolecular composites (MIC) materials. The goals were to obtain an improved understanding of flame propagation mechanisms and combustion behaviors associated with nano-structured energetic materials. Information on issues such as reaction rate and behavior as a function of composition (mixture ratio), initial static charge, and particle size are essential and will allow scientists to design applications incorporating the benefits of these compounds. The materials have been characterized, specifically focusing on particle size, shape, distribution and morphology.

INTRODUCTION

The term thermite reaction is used here to describe an exothermic reaction which involves a metal reacting with a metallic or a non-metallic oxide to form a more stable oxide and the corresponding metal or nonmetal of the reactant oxide.[1] Thermite reactions have long been used in a variety of pyrotechnic, material synthesis, and metallurgical applications.[1] These materials are potentially attractive because the reactions are highly exothermic, have high energy densities, and high temperatures of combustion. However, their use has been limited because their energy release rate is typically relatively slow. In recent years it has been demonstrated that considering reactants on the nano-scale reduces the diffusion barrier sufficiently to dramatically increase the energy release rate.[2] In a sense, the rules are changed at the nano-scale and a door is opened for the consideration of new applications for these materials. Engineered nano-scale composite energetic materials, such as Al/MoO_3, have shown promise for energetic material applications because the nanocomposite can react extremely rapidly. Reaction rates are orders of magnitude faster than conventional formulations.[2] As a consequence these materials have application directly for such things as primers, or nano-materials can be formulated with other energetic materials, including gas generating materials, and used for a much wider variety of applications. These materials have been historically termed metastable intermolecular composites (MIC). Here we use this term to refer to any energetic material utilizing nanoscale energetic constituents.

Although these materials have been available in the recent years, much research remains to fully characterize the morphology and reaction behavior of these materials..

Fully characterizing these materials presents challenges. Small angle neutron or x-ray

scattering (SANS and SAXS, respectively) is introduced and shown to be a useful characterization tool for these nano-materials to characterize size distribution and oxide layer thickness. Other size characterization tools and their range of useful resolution are presented in Fig. 1. This figure shows that SAXS and SANS span the range of interest for nanoscale materials.

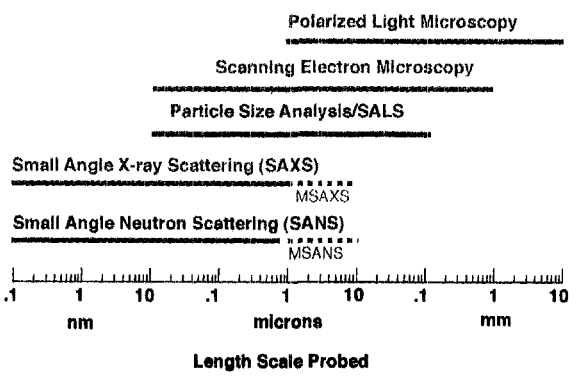

Figure 1. A comparison of particle characterization techniques in terms of length scale probed.

In this paper, we present recent combustion experiments involving Al/MoO_3 and Al/MoO_3/Teflon MIC materials. Ignition delay and pressurization are measured in a small-volume combustion bomb. Variations in the performance of the materials are contrasted. Corresponding characterization of the materials studied is also shown.

EXPERIMENTAL SETUP

There are many methods for preparing nanocomposite thermites, including sol-gel synthesis[4] deposition of individual fuel and oxidizer layers that make up a multi-layer foil[5] and sonication of suspended particulates.[2] For this study, Al and MoO_3 powders were immersed in a solvent and sonicated. The particles were suspended in the solvent and once thoroughly mixed, the mixture was poured into a pan and heated to a few degrees above ambient, allowing the solvent to evaporate.

We have considered both the morphological characterization and combustion of these materials. The Al and MoO_3 powders were characterized using several different techniques to determine the particle size distribution, passivation layer thickness, and degree of particle agglomeration. In this paper we present results from pressure cell experiments and pellet burning experiments.

SANS/SAXS Measurements

Small-angle neutron scattering (SANS) measurements were performed on Al and MoO_3 powders used to make MIC materials, in order to characterize their particle size and shape. In what follows, we will briefly describe the SANS technique. A much more detailed description of the SANS and SAXS measurements is presented in by Peterson et al. in this volume.[8]

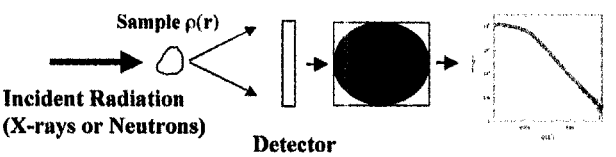

Figure 2. Schematic of small-angle scattering technique.

In a SANS experiment, a beam of neutrons impinges upon a sample characterized by a scattering length density, $\rho(\mathbf{r})$, which reflects the microscale structure (see Fig. 2). Fluctuations in $\rho(\mathbf{r})$ give rise to small-angle scattering. The intensity of the scattered radiation, $\mathbf{I(Q)}$, is measured as a function of the scattering vector, $\mathbf{Q}$, of magnitude $Q = (4\pi/\lambda)\sin\theta$, where λ is the wavelength of the incident radiation and θ is half of the scattering angle. $\mathbf{I(Q)}$, for a monodisperse system of non-interacting particles, dispersed in a uniform media, can be expressed as,

$$I(Q) = N\Delta\rho^2 V^2 \langle P(\mathbf{Q}) \rangle, \qquad (1)$$

where $P(\mathbf{Q})$ is the normalized, single particle form (shape) factor and is related to Fourier transform of $\rho(\mathbf{r})$, V is the particle volume, and N is the number of scatterers per unit volume. Also, $\Delta\rho$ is

the scattering length density contrast between the average scattering length density of the particle, and that of the surrounding media. The complete interpretation of **I(Q)** in terms of the sample structure, $\rho(\mathbf{r})$, ultimately involves careful comparison with calculations of the scattering expected from model structures. However, useful characteristics of the scattering, based on approximations to Eq. (1), can be used to determine general features of the structure. For example, for a collection of objects of a characteristic feature size, in the domain such that $QR \approx 1$, where R is the feature size, one observes a *knee* in a log-log plot of the intensity versus Q, known as the Guinier region.

Other assumptions can also be made, as determined from the data itself and verified by SEM images. A significant advantage of SANS or SAXS is that a statistically significant number of particles is sampled in a single measurement, which allows accurate assessment of particle size distributions. SANS measurements were performed on the Low-Q Diffractometer (LQD) at the Manuel Lujan Jr., Neutron Scattering Center. Data were reduced by conventional methods and corrected for empty cell and background scattering. Absolute intensities were obtained by comparison to a known standard and normalization to sample thickness. SAXS measurements have been made at the University of New Mexico, and a new SAXS facility is nearly operational at Los Alamos.

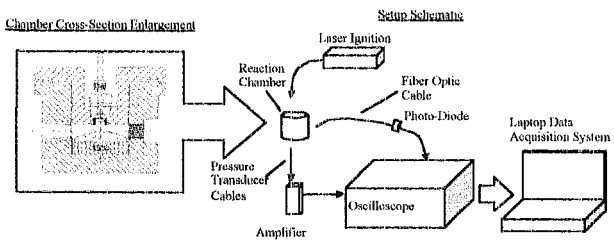

Figure 3. Schematic of pressure cell experiment. The sample is ignited by Nd:YAG laser. Pressure transducer record the pressurization and a photodiode records light emission. Powders or pellets can be considered.

Pressure Cell Experiment

Figure 3 is a schematic diagram of a constant volume (13 cc), cylindrical chamber. Pressure and light intensity were measured in this constant volume chamber during the reaction. A fixed volume of powder was placed in the chamber and laser ignited. Ignition occurred via a fiber-optic cable by a 30 ns, 20 mJ pulse from a Nd:YAG laser. Two PCB Piezotronics[INC.] high-frequency pressure transducers were installed in the wall of the chamber; one with a 50 psi range and the other with a 250 psi range. These transducers fed a voltage signal to a digital Tektronics oscilloscope via a signal amplifier. A fiber-optic cable mounted in the wall of the chamber monitored light emission from each test. The light signal from the cable was transformed into a voltage signal by a photo-diode and then sent to the oscilloscope. The voltage-versus-time data was collected and processed with a laptop computer with data acquisition capabilities.

Pellet Combustion Experiment

Pellets of Al/MoO_3 MIC where produced in an axial press of about 4.4 mm diameter and about 5 mm in length. Various density pellets can be obtained. The lower density pellets (<2.4 g/cc) generally exhibit nonplanar burning. Presumably, small unobserved flaws are accessed and flames spread rapidly through the pellet. This is very similar to the combustion of energetic materials where nonplanar convective burning can be observed in damaged material at pressures sufficient for flame incursion. Flame spreading down the side of pellets is also sometimes observed.

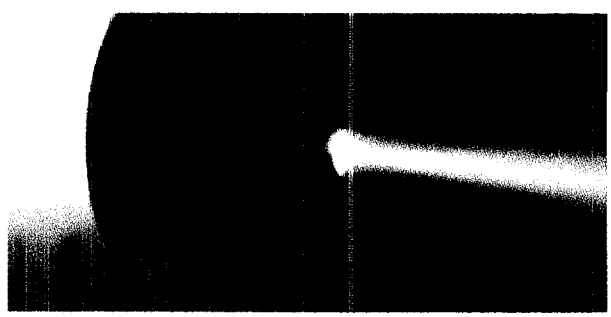

Figure 4. Combustion of a lower density pellet that has been coated with a thin coat of epoxy.

Initially, we tried applying a thin coat of epoxy to the sides of the pellet, which is the usual method of inhibiting side burning of pellets or

strands of energetic materials. This inhibited flame spread on the sides of the pellet, however the epoxy apparently mixed with a small amount of MIC material to create an extremely opaque layer so the intense burn front could not be observed.

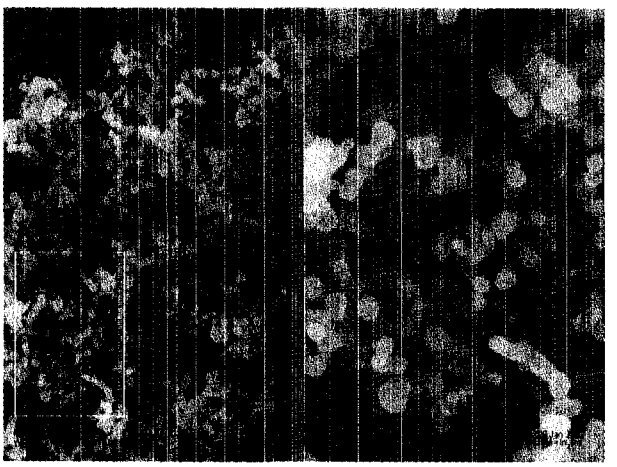

(a)

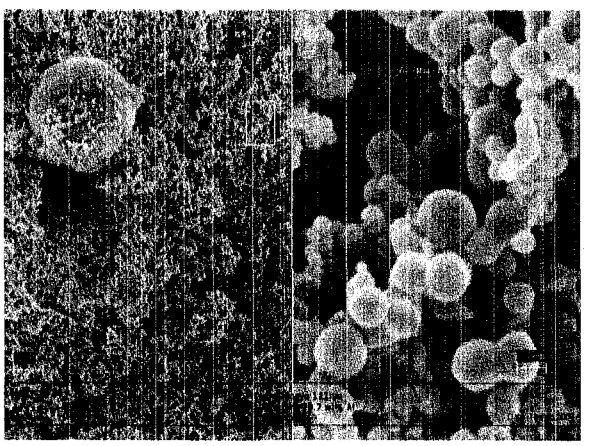

(b)

Figure 5. Part (a) is a SEM image of nano-aluminum made at Los Alamos, designated RF-B. Part (b) is larger aluminum made by Technanogy, designated Technanogy-121. Technanogy also makes small aluminum powders similar to RF-B shown in part (a). The particle size distribution tends to widen as larger particles are formed.

Both of the above effects are illustrated in Fig. 4 where the burning front cannot be seen through the epoxy layer and flame has spread through to the bottom the pellet and is jetting hot products. We found that spraying a very thin layer of polyurethane adequately inhibited side flame spread, yet allowed observation of the flame front. Igniting the entire pellet surface initially is also important. We were able to accomplish this adequately by illuminating the entire surface with a Nd:YAG laser. A planar burning MIC pellet is presented below.

CHARACTERIZATION OF MATERIALS

SEM Results

Figure 5 shows an SEM for typical aluminum samples. As illustrated in this figure, our experience is that the size distribution widens as larger particles are obtained for materials we have considered. Also observed in part (a) of Fig. 5, we see agglomeration in the form of chains or branches. This is consistent with small-angle scattering results. Similarly, Fig. 6(a) is MoO_3 and finally Fig. 6(b) is Al/ MoO_3 MIC. The MoO_3 images reveal sheet-like structures, intermixed with aggregates. The SAXS results agree with the SEM images and provide a quantitative measure of sheet thickness as discussed below.

SANS/SAXS Results

Figure 7 shows data obtained from SAXS measurements of MoO_3 and Al (LA-Al31500). Data obtained from a sample of Climax MoO_3 and the model fit of polydisperse sheet-like structures with large aggregates is shown in Fig. 7(a). The model assumption is consistent with the SEM shown in Fig. 6(a). Specifically, sheet-like structures with large aggregates are observed in the SEM images, and if this structure is assumed to fit the SAXS measurement, good agreement is achieved with the small-angle scattering data. This analysis yields a sheet thickness of 15.5 nm. Figure 7(b) is a comparison of size distributions of an Al powder obtained from a SAXS measurement and TEM images. The comparison is reasonable considering the limitations of the sample size considered in the TEM measurements (only a few hundred particles), possible halo effect (electron diffraction) in the TEM images, and the difficulty determining the diameter of agglomerates. In contrast, the SAXS measurement includes numerous particles.

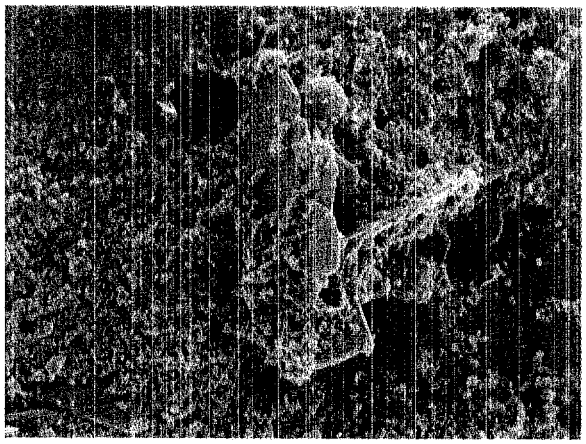

(a)

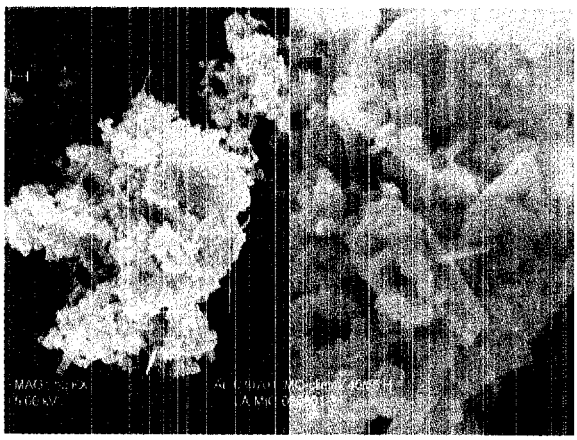

(b)

Figure 6. Part (a) is some MoO3 from Climax. Sheet-like material is observed with smaller particles. Part (b) is Al/MoO3 MIC.

Powder	Fractal Dimension	R_{avSR} (core) (nm)	R_{avSV} (core) (nm)	D_{avSR} (nm)	D_{avSV} (nm)	BET D_{av} (nm)	TEM D_{avSR} (nm)	δ (nm)	TEM δ (nm)	BET/ TGA δ (nm)	Vol. δ (nm)
Al-31500	1.98 ± 0.1	10.4 ± .1	12.9 ± .1	26.2 ± 0.2	31.2 ± 0.2	32.90	39.83	2.68 ± 0.02	2.83	2.45	2.87
Al-13100	1.7 ± 0.2	10.6 ± .2	25.4 ± .3	26.1 ± 0.4	54.9 ± 0.6	34.15	40.20	2.44 ± 0.02	4.62	2.45	2.98
Al-RF-B	1.8 ± 0.1	10.4 ± .1	18.7 ± .1	26.5 ± 0.2	43.1 ± 0.2	-	-	2.86 ± 0.02	-	-	-

Table 1. Sizing of aluminum core and oxide layer by various techniques.

In Figure 8 we show the distribution obtained from a SANS measurement of three Los Alamos produced nano-aluminums. Mass fractal agglomerates are assumed in the interpretation of the scattering, consistent with SEM images (see Fig. 5(a) for example). This model was found to be consistent with the SANS data in that the assumption of mass fractal agglomerates matched the data well. Both particle number distribution and volume distribution are shown in the figure. Table 1 shows sizing results from SANS with comparisons to other approaches. In Table 1, R_{av} is the average radius, D_{av} is the average diameter, and δ is the oxide layer thickness.

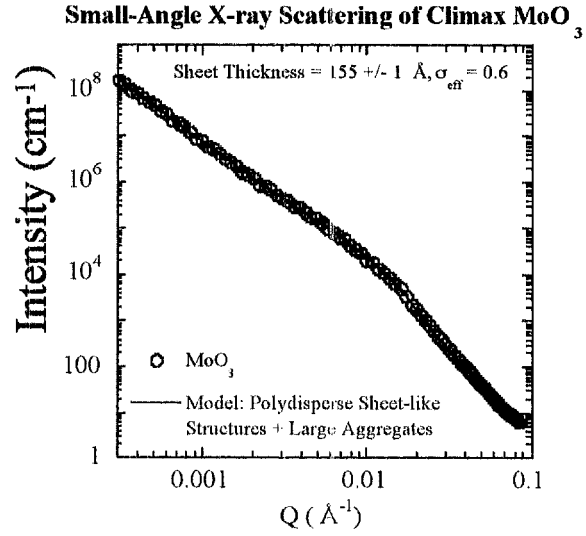

(a)

Method	Mean Diameter (nm)	Mean Oxide Layer Thickness (nm)
TEM	40 +/- 8	2.8 +/- 0.5
SAXS, Gaussian Distrib.	31.3 +/- 0.3	2.0 +/- 0.1
SAXS, Lognormal Distrib.	32.1 +/- 0.2	2.3 +/- 0.1

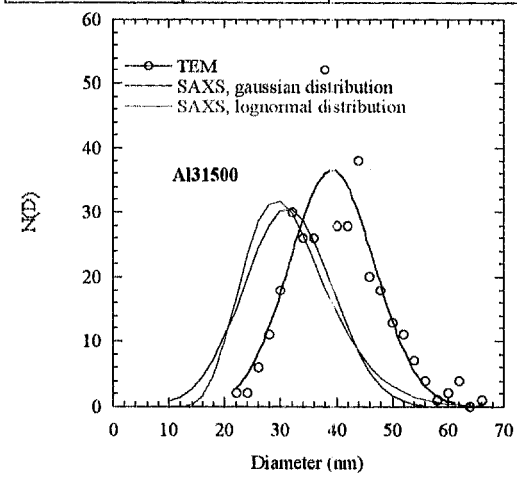

(b)

Figure 7. Part (a) is data obtained from a sample of Climax MoO3 and the model fit of polydisperse sheet-like structures with large aggregates (consistent with Fig. 6a). This yields a sheet thickness of 15.5 nm. Part (b) is a comparison of size distributions obtained from a SAXS measurement and TEM images.

PRESSURE CELL EXPERIMENTS

The pressure cell experiment, as described above, was used to compare powder samples of MIC materials. Samples are placed in the same volume for each experiment. It must be noted that the density can vary because of the different bulk powder densities. However, the density is determined for each test since sample mass is measured and the sample volume is fixed. Typical traces are shown in Fig. 9 (a). Ignition time is defined as the time required for the reaction to produce 5% of the maximum pressure. This time is measured from the initial laser pulse. This parameter is indicative of the reactivity of the material. The maximum pressurization rate is determined from the slope of the pressure versus time plot during rapid pressurization. Good repeatability is obtained with this experiment as illustrated in Fig. 9 (a) by the overlaying pressure traces.

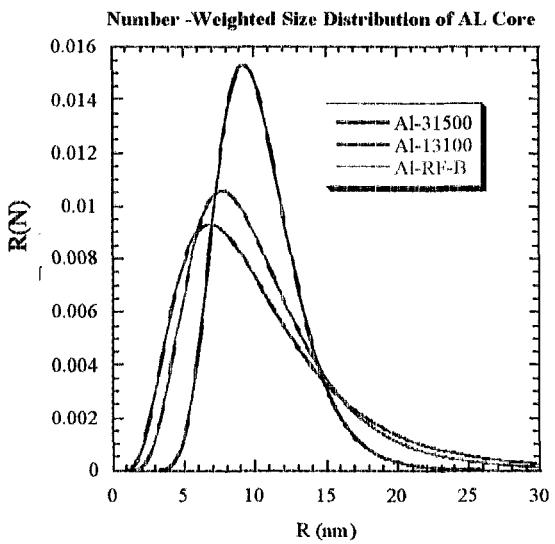

Figure 8. Size distributions of three Los Alamos aluminum samples.

Effect of electrostatic Charge

Nano-composite Al/MoO_3 mixtures exhibit high spark-sensitivity, especially in dry environments. This phenomenon led to questions about the possible effect of electrostatic charge on material ignition behavior. Consequently, a series of tests were conducted in the pressure cell to quantify possible performance variations caused solely by electrostatic charge. The composition of the mixture and the origins of the Al and MoO_3 were held constant. Seven mixtures with different charges were examined. The first two mixtures were not altered, the third and fourth were neutralized with a destatic gun. An attempt was made to positively charge the fifth and sixth samples, while the seventh sample received a negative charge, both using the destatic gun in either only the positive or negative mode. The average density of the powder for all mixtures was 0.126 ± 0.006 g/cm^3.

Figure 9 (b) shows that no significant

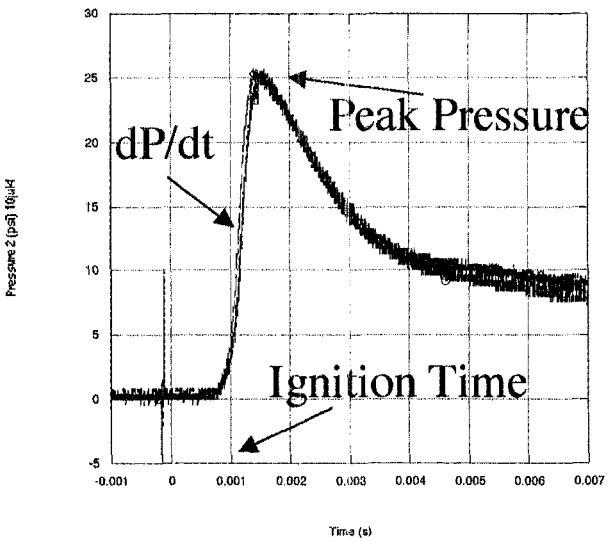

(a)

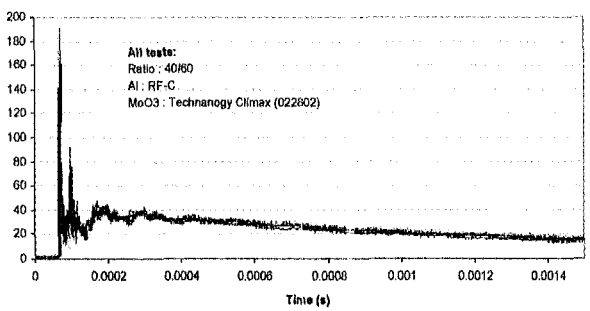

(b)

Figure 9. In part (a) typical pressure traces illustrate the repeatability and the quantitative metrics obtained from the pressure traces for comparisons. Part (b) is several test of the same material with different static charge induced.

variations of any of the major performance characteristics (i.e., ignition delay, pressurization rate, and peak pressure) were evident as a function of the electrostatic charge on the powder. The pressure histories of all seven tests overlaid consistently. These results imply that the electrostatic charge on the sample does not appear to play a significant role in the overall performance of the material. Potentially, there might be an effect on the spark sensitivity. Unfortunately, our spark test does not allow variation of the input spark so this could not be determined.

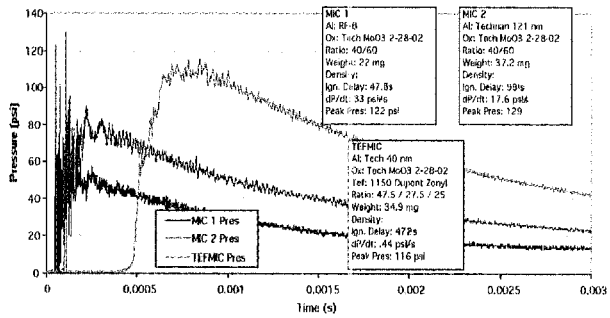

Figure 10. Comparisons of three types of MIC compositions in the pressure cell test.

Aluminum Size & the Addition of Teflon Effects

When the aluminum size is changed, an effect on the reaction performance is expected. In Fig. 10 we changed the aluminum from a small size (LA-Al-RF-B, see Fig. 8 for size distribution) to larger aluminum (Techanogy-121, see Fig. 5 (b) for size characterization). There were measurable differences in the ignition times and maximum pressurization rate, as shown in the figure caption. However, we note that the weight of material (density) differed significantly. That may affect some of the differences observed as well as the higher and longer pressure trace of the denser and larger aluminum particle MIC. In Figure 11 we compare the pressure response of two materials that are more similar than those in the previous example. This figure illustrates how the performance differences are nearly indistinguishable between the two Al/MoO_3 mixtures. In these two mixtures, the Al particles were slightly different (see Fig. 8 for size distributions), but the MoO_3 and composition ratios were held constant. The density differences alone may account for the differences observed. Open burns (see Son et al.[6] for more details of the open burn experiment) gave similar results. Specifically for the LA-Al-RF-B MIC we obtained 362 and 376 m/s for two runs. For the LA-Al-031500 MIC we measured 410 and 413 m/s for two runs.

Formulating with various materials can affect the ignition and sensitivity significantly. Tepper and Kaledin[7] found that the doping kerosene with nano-Al particles causes significant decreases in ignition delay times. This has important implications in super-sonic propulsion systems where mixing lengths are long. Shorter ignition delays lead to smaller propulsion systems. Nano-particle size was not examined in Tepper's study; however, our observations imply that reducing particle size may additionally contribute to decreasing the ignition delay time. The Al/MoO_3/Teflon mixture generates more gas than MIC without Teflon. Using Teflon as a gasifying agent causes the pressure history to naturally exhibit higher pressure sustained over a longer duration, as observed in the pressure traces in Fig. 10.

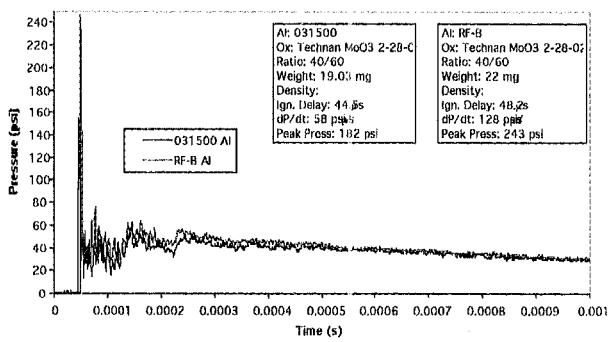

Figure 11. Comparison of two similar MIC compositions.

Mixture Ratio Effect

Changing the stoichiometry is expected to affect the propagation rate significantly. This is confirmed in Fig. 12 where the percentage of aluminum was varied and both open loose powder burn propagation rate and maximum pressurization rate is presented. Relatively small changes in the percentage of aluminum have large effects on the propagation rate and pressurization rate. In fact, the percentage of aluminum was varied by only 14% in the figure. As might be expected, there is a clear correlation between the propagation rate and the pressurization rate in the figure. The burning powder pressurizes the cell. If the propagation rate is faster, the pressurization rate would be expected to be faster.

PELLET COMBUSTION EXPERIMENTS

Density Effect

As mentioned in the experimental section, Al/MoO_3 MIC pellets exhibit nonplanar burning at lower densities. Our interpretation is that when flaws exist in the pellets flames can spread in and spread convectively through the pellet. Convective burning in loose powders or lower density pellets appears to be the dominant propagation mechanism.[6] The MIC pellets burn much more rapidly than other energetic materials. Consequently, we were concerned about igniting the entire face of the pellet nearly simultaneously. This was achieved using laser ignition with the beam spread across the entire face. At higher densities, planar normal burns were achieved. A picture of one such burn is shown in part (b) of Figure 12. The density of this pellet was 2.93 g/cc. The burn rate was measured at 20.6 cm/s. This rate is three orders of magnitude slower than the propagation rate observed in the loose powder. This is consistent with the transition from convectively dominated burning to conductive (or normal deflagration) burning. This propagation rate is about two orders of magnitude faster than HMX burning at one atmosphere and an order faster than the faster burning organic energetic material under the same conditions. We anticipate further studies at different pressures and particle sizes. The laser used was not sufficient to ignite an Al/MoO_3 MIC pellet that used Techanogy-121 aluminum. We have observed that ignition is more difficult when the MIC is pressed compared to loose powders and the above results show differences in the ignition delay between the smaller and larger particle-sized MIC materials.

CONCLUSIONS

This paper reported initial studies of the ignition and combustion of MIC materials. Results of the effect on ignition and reaction as a function of particle size, composition (mixture ratio), initial electrostatic charge, and particle size was presented. SEM, SANS, and SAXS characterization data was presented. Small-angle scattering is shown to be an appropriate and useful tool in the characterization of these materials.

ACKNOWLEDGEMENTS

We acknowledge the support of Los Alamos National Laboratory, under contract W-7405-ENG-36. In particular, we acknowledge the support of the DoD/DOE MOU program of Los Alamos National Laboratory. We acknowledge Harriet Kung for the TEM size measurements also.

REFERENCES

1. L. L. Wang, Z. A. Munir, Y. M. Maximov, *Journal of Material Science*, 28:3693-3708 (1993).

2. C. E. Aumann, G. L. Skofronick, and J. A. Martin, *Journal of Vacuum Science & Technology* B 13(2): 1178-1183 (1995).

3. T. Lowe, *Advanced Materials & Processes*, pp. 63-65 (2002).

4. A.E. Gash, R.L. Simpson, T.M. Tillotson, J.H. Satcher, and L.W. Hrubesh, *The Twenty-Eighth International Pyrotechnics Seminar*, Colorado (2000).

5. A.B. Mann, A.J. Gavens, M.E. Reiss, D. Van Heerden, G. Bao, and T.P Weihs., *J. Appl. Phys.* **82**(3), 1178-1188 (1997).

6. S. F. Son, H. L., B. W. Asay, J. R. Busse, B. S. Jorgensen, B. Bockmon , and M. Pantoya,

"Reaction Propagation Physics of Al/MoO_3 Nanocomposite Thermites," The International Pyrotechnics Society, The Twenty-Eighth International Pyrotechnics Seminar, Adelaide, Australia, November 4-9, 2001.

7. F. Tepper, and L. A. Kaledin, "Nano Aluminum as a Combustion Accelerant for Kerosene in Air Breathing Systems," AIAA-2001-0521, (2001).

8. P. D. Peterson, J. T. Mang, S. F. Son, B. W. Asay, M. F. Fletcher, and E. L. Roemer, "Microstructural Characterization of Energetic Materials," These proceedings, 2002.

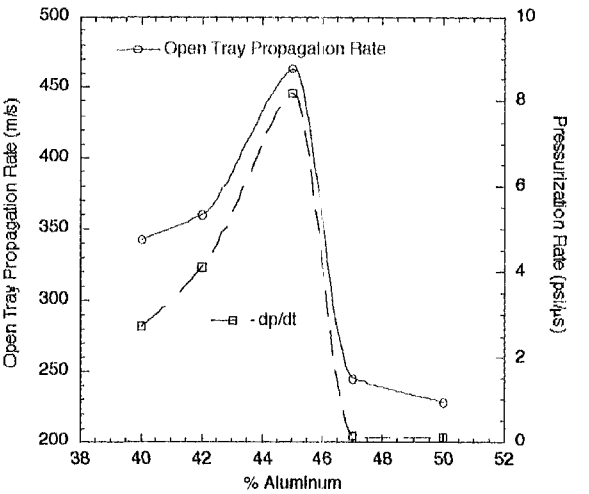

(a)

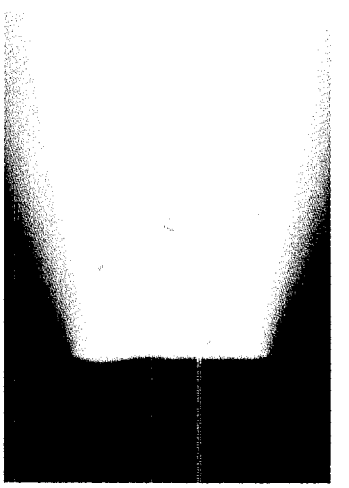

(b)

Figure 12. Part (a) shows the dependence of the percent of Al on the maximum pressurization rate and open tray burn. Nano-Aluminum from Nanotechnology was used. Part (b) shows a burn of a high density pellet (2.9 g/cc). Normal planar burning was observed.